nature communications

Article

https://doi.org/10.1038/s41467-025-58355-8

Circularly polarized luminescence with high dissymmetry factors for achiral organic molecules in solutions

Received: 13 December 2024

Accepted: 18 March 2025

Published online: 26 March 2025

Check for updates

Ming-Jun Ji[1,2,3], Wen-Long Zhao[1,2,3], Meng Li[1,2] ✉ & Chuan-Feng Chen[1,2] ✉

Circularly polarized luminescence (CPL) in solution offers several advantages. However, it remains challenging for organic molecules to achieve circularly polarized luminescence with high dissymmetry factor (g_{lum}) in solution. Herein, a general strategy is developed by placing chiral nematic liquid crystals (N*-LCs) behind the solution of achiral organic molecules. The selective reflection-transmission mechanism of solution-N*-LC composite system enables the generation of full-color and white circularly polarized light with $|g_{lum}|$ even reaching 2.0. This strategy demonstrates versatility, being applicable to both aqueous and organic solutions, and effectively achieving the circularly polarized luminescence of multiple molecules with high g_{lum} values. Additionally, CPL switching and logic gate applications are successfully realized by leveraging the selective reflection-transmission mechanism of N*-LCs and the reversible acid-base responsiveness of the solution systems. This work provides a general and robust strategy for achiral organic molecules to achieve circularly polarized luminescence with high $|g_{lum}|$ values in solutions.

Circularly polarized light (CP light) is a kind of electromagnetic wave with constant amplitude[1–3]. In recent years, due to its optical properties, circularly polarized luminescence (CPL) matrerials has wide potential applications in fields such as 3D displays, optoelectronic devices, chiral sensors, and anti-counterfeiting technologies[4–10]. One of the most significant properties of CPL is the dissymmetric luminescence factor, denoted as g_{lum}. The definition of this factor is given by the equation $g_{lum} = 2(I_L - I_R)/(I_L + I_R)$, where I_L represents the emission intensity of left-handed circularly polarized light and I_R denotes the emission intensity of right-handed circularly polarized light. According to this definition, the theoretical values of $|g_{lum}|$ can range from 0 to 2[11]. However, the low g_{lum} value of early circularly polarized luminescent materials have limited their practical applications. Therefore, to achieve circularly polarized luminescence with higher g_{lum} values in micro- or macromolecules, researchers commonly employ chiral strategies, which typically involve covalently bonding chiral components to luminescent molecules, resulting in a substantial body of research[12–20]. Among them, circularly polarized luminescence in solution systems offers several advantages, including higher sensitivity, reduced influence from light reabsorption and scattering, more consistent molecular orientation, more uniform molecular dispersion, and potential biomedical applications[21]. However, due to the reduction in the degree of chiral assemble or the appearance of monomeric states in solution, the $|g_{lum}|$ values of chiral organic luminescent molecules solutions typically ranges only from 10^{-4} to 10^{-3}[22–26]. Moreover, the synthesis of chiral organic luminescent molecules usually requires complex chiral resolution processes, contributing to their high costs. Therefore, developing a general strategy to achieve efficient circularly polarized luminescence with high $|g_{lum}|$ values in solutions of achiral organic luminescent molecules remains an important and challenging task.

Liquid crystals (LCs) occupy a thermodynamic state between an organized crystalline solid phase and a completely disordered isotropic liquid phase[27–29]. They exhibit a state of order reminiscent of solids while retaining the fluidity of liquids. By introducing chiral dopants into LCs, chiral nematic liquid crystals (N*-LCs) can be

[1]Beijing National Laboratory for Molecular Sciences, CAS Key Laboratory of Molecular Recognition and Function, Institute of Chemistry, Chinese Academy of Sciences, Beijing, China. [2]University of Chinese Academy of Sciences, Beijing, China. [3]These authors contributed equally: Ming-Jun Ji, Wen-Long Zhao. ✉e-mail: limeng@iccas.ac.cn; cchen@iccas.ac.cn

formed[30–33]. In recent years, researchers have leveraged the co-assembly of N*-LC hosts with chiral or achiral luminescent guest molecules, effectively amplifying or generating CP light with significantly enhanced g_{lum} values through the selective reflection-transmission mechanism of the liquid crystals[30,33–49]. These co-assembly strategies of N*-LC include the ternary co-assembly of achiral luminescent molecules - chiral dopants - liquid crystals, binary co-assembly of chiral luminescent molecules - achiral liquid crystals, binary co-assembly of achiral luminescent liquid crystals - chiral dopants, and binary co-assembly of chiral liquid crystals - achiral luminescent molecules. These approaches undoubtedly address the challenge of achieving $|g_{lum}|$ values greater than 1 in the aggregated and solid states for circularly polarized luminescence. However, the $|g_{lum}|$ values in these co-assembly systems are difficult to further improve to 2. This is likely due to the uneven dispersion of luminescent molecules within the N*-LC system and the disruption of the highly ordered chiral assembly of the N*-LCs caused by the addition of luminescent molecules.

Inspired by these work, to achieve circularly polarized luminescence with high $|g_{lum}|$ values in solution from achiral organic molecules and to verify whether the separation of luminescent molecules from N*-LCs can further enhance $|g_{lum}|$ values, we herein propose a general and robust strategy. In this strategy, the achiral luminescent molecules were separated from N*-LCs and the N*-LCs were placed behind the solution of achiral luminescent molecules (Fig. 1). Notably, it is found that the $|g_{lum}|$ values of these composite systems can all exceed 1.5 and, in some cases, approach 2. This strategy is highly versatile. It is applicable to a range of molecular types, including non-chiral fluorescent, phosphorescent, and thermally activated delayed fluorescence (TADF) molecules. Additionally, this strategy can generate full and white color CP light with high $|g_{lum}|$ values in both aqueous and organic solutions.These results also demonstrate that when achiral molecules are separated from N*-LCs, the absence of issues such as uneven dispersion of achiral molecules within the N*-LCs and the disruption of the ordered chiral assembly of N*-LCs by the achiral molecules, allows this strategy to further enhance the $|g_{lum}|$ values of the N*-LC-based composite systems for circularly polarized luminescence. Morover, in this work, a molecular logic gate based on circularly polarized luminescence was successfully designed by leveraging the reversible stimulus-responsive mechanism of luminescent color changes in solution and the selective reflection and transmission mechanisms of N*-LC.

Results

Preparation and characterization of N*-LC

Doping chiral dopants into liquid crystals is a widely adopted method for preparing N*-LCs[30–33]. Herein, a series of N*-LC materials (**R1**–**R9, S1**–**S9**) with varying chiral dopant ratios were prepared by doping *R/S*-5011 into SLC1717 (Supplementary Tables S1, S2). These N*-LCs were then encapsulated between two quartz plates, and their photophysical properties were investigated using polarized optical microscopy (POM), UV-vis absorption spectroscopy, circular dichroism (CD) spectroscopy, reflection-transmission spectroscopy, and CPL spectroscopy. POM of *R*-type N*-LCs was employed as example to examine the texture of the prepared N*-LCs (Fig. 2a–c, Supplementary Fig. S3). The results of POM confirm the excellent compatibility of *R*-5011 with SLC1717 and the successful construction of the cholesteric phase. Furthermore, the classical oily streak textures observed in the POM images suggest that the helical axes of the prepared N*-LCs are oriented perpendicular to the quartz substrate[30,50]. UV-vis absorption and CD spectroscopy are among the most effective and widely used techniques for studying the chiroptical properties of compounds. Supplementary Figs. S1, S2, S4, and S5 present the UV-vis and CD spectra of the prepared N*-LCs. The UV-vis and CD spectra feature two peaks: the first, located at 330 nm, corresponds to the absorption of *R/S*-5011[16,51]; while the second, attributed to the N*-LCs, shifts with varying *R/S*-5011 doping ratios. Notably, distinct CD signals are observed at the absorption peaks of N*-LC in the CD spectra of **R1**–**R9** and **S1**–**S9**, owing to the formation of chiral co-assembled structures. *R*-type N*-LCs consistently exhibit negative CD signals, whereas *S*-type N*-LCs

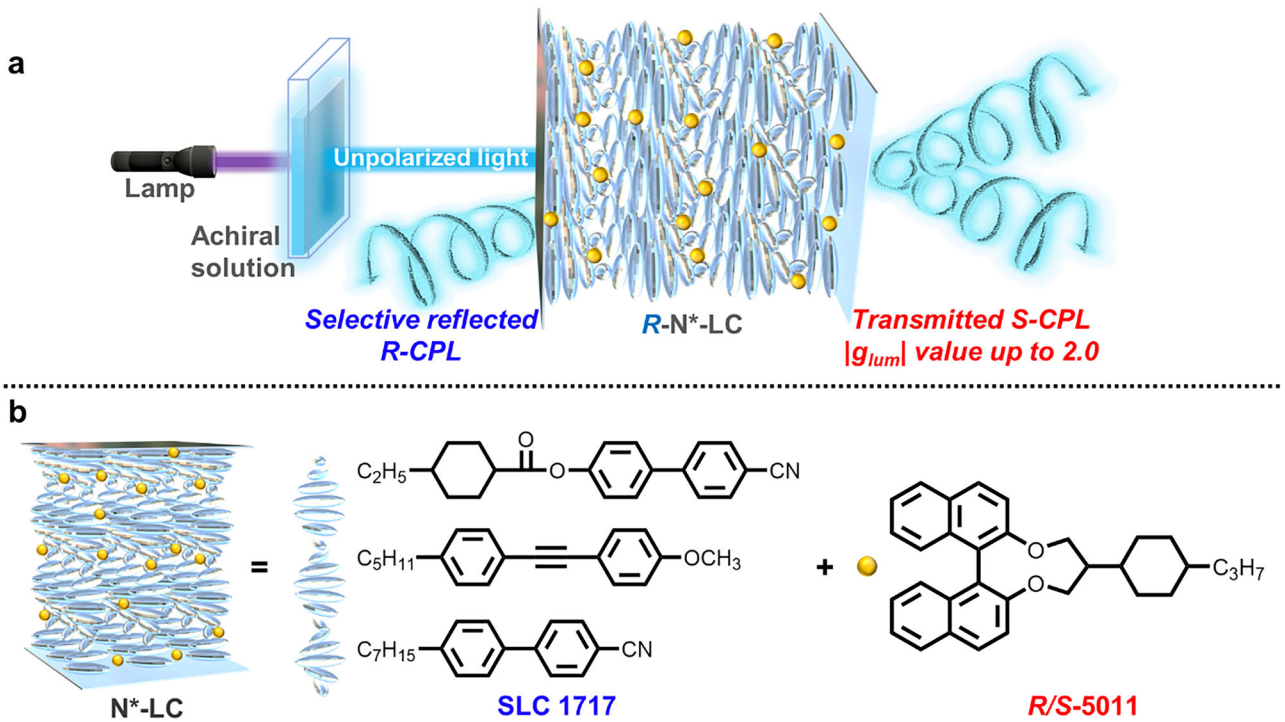

Fig. 1 | The schematic of the strategy proposed in this study. a The selective reflection and transmission mechanism of N*-LCs. **b** The composition of the prepared N*-LCs in this study.

https://doi.org/10.1038/s41467-025-58355-8

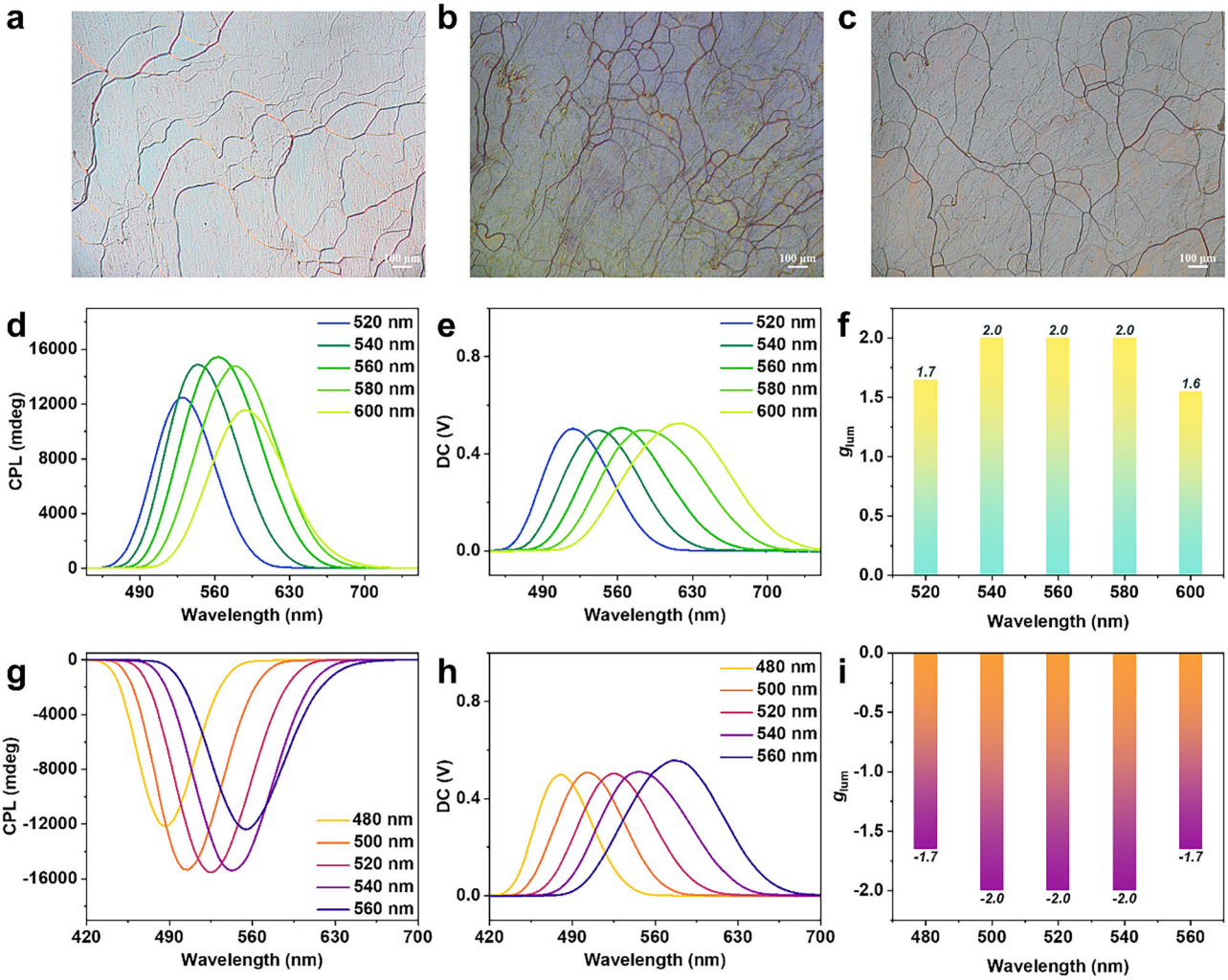

Fig. 2 | Spectrum of N*-LCs. POM images of **a** R4, **b** R7 and **c** R8, **d** CPL, **e** DC and **f** g_{lum} values of circularly polarized light generated after unpolarized light of different wavelengths passes through **R7**. **g** CPL, **h** DC and **i** g_{lum} values of circularly polarized light generated after unpolarized light of different wavelengths passes through **S7**.

display positive CD signals. Importantly, the CD intensities of all N*-LCs either approach or exceed the instrumental limit of ±30,000 mdeg, indicating a successful transfer of chirality from *R*/*S*-5011 to the N*-LCs.

The chiroptical properties and ground-state chirality of the prepared N*-LCs was confirmed through UV-vis and CD spectroscopy, indicating their potential to convert unpolarized light into circularly polarized light. It is well-established that the generation of high dissymmetry factors in CPL from N*-LCs is attributed to their selective reflection and transmission mechanisms. Specifically, when an unpolarized light with a wavelength matching the selective reflection/transmission band of a N*-LC passes through the N*-LC material, it is split into two circularly polarized light with opposite handedness. Among these, the circularly polarized light with the same handedness as the N*-LC is selectively reflected, while the opposite-handed component is transmitted and detected[30,52]. Therefore, according to the definition of the dissymmetry factor, $g_{lum} = 2(I_L - I_R)/(I_L + I_R)$, this mechanism theoretically enables the generation of CP light with g_{lum} values reaching the theoretical maximum of ±2. To validate this, the reflection and transmission spectra of the prepared N*-LCs and the CPL properties of light transmitted through the N*-LCs at different wavelengths were all systematically measured (Supplementary Tables S3, S4, Supplementary Figs. S6–S27). In terms of spectral peak positions, consistent with the UV-vis and CD spectra, the reflection and transmission peaks of the N*-LCs shift with changes in doping ratio. Moreover, for each specific N*-LC, the spectral peaks in the UV-vis, CD, reflection, and transmission spectra can be directly correlated. CPL measurements show that unpolarized light passing through *R*-type and *S*-type N*-LCs generates left-handed and right-handed circularly polarized light, respectively. Furthermore, the CPL results reveal a clear correlation between the wavelength of the incident unpolarized light and the resulting CPL properties. Specifically, when the wavelength of the unpolarized light approaches the reflection/transmission peaks of the N*-LC, the CPL signal and dissymmetry factor increase even reaching the theoretical maximum value of ±2 for circularly polarized light. Conversely, as the wavelength of the unpolarized light moves away from the reflection/transmission peaks, both the CPL signal and dissymmetry factor decrease. For example, the reflection spectrum of **R7** exhibits a peak around 560 nm. Therefore, when an unpolarized light with a wavelength near 560 nm passes through **R7** via its selective reflection-transmission mechanism, left-handed circularly polarized light with a dissymmetry factor of 2 can be obtained. As the wavelength of the non-polarized light deviates from 560 nm, with the DC intensity remaining constant, both the CPL signal intensity and the g_{lum} value gradually decrease. At unpolarized light wavelengths of 520 nm and 600 nm, the g_{lum} value decrease to 1.7 and 1.6, respectively (Fig. 2d–f, Supplementary Fig. S16). Similarly, for **S7**, its reflection spectrum shows a peak around 520 nm. Consequently, when 520 nm unpolarized light passes through **S7**, right-handed circularly polarized light with a dissymmetry factor of -2 is generated. As the wavelength of the light shifts away from 520 nm, the CPL signal and $|g_{lum}|$ value

gradually decrease, with g_{lum} value reaching −1.7 at 480 nm and 560 nm (Fig. 2g–i, Supplementary Fig. S25). Through this comprehensive series of CPL measurements, demonstrated the potential of these N*-LC to convert unpolarized light into circularly polarized light with high dissymmetry factors.

Circularly polarized luminescence of solution-N*-LC composite system

After confirming that the prepared N*-LCs possess the potential to convert unpolarized light into circularly polarized light with high dissymmetry factors, a general strategy for achieving circularly polarized luminescence with high dissymmetry factors in achiral solutions was proposed. The achiral luminescent molecules are first employed to generate unpolarized light with varying wavelengths in solution. Next, N*-LCs with selective reflection-transmission spectra that match the emission wavelengths of solutions are selected and placed behind the achiral solution. Through the selective reflection and transmission processes of the N*-LCs, the unpolarized light generated by the achiral solution is transformed into circularly polarized light with high dissymmetry factors (Fig. 3). To validate the feasibility of this strategy, 4-methylumbelliferyl phosphate disodium (4-MUP, Fig. 3), an achiral, water-soluble fluorescent substrate for phosphatase detection, was first dissolved in aqueous solution for testing. In aqueous solution, the fluorescence emission spectrum of 4-MUP is shown in Supplementary Fig. S34. Following the strategy proposed in this work, the emission spectrum of 4-MUP in aqueous solution was compared with the reflection spectra of various N*-LCs. The results revealed that the **R1** and **S1** N*-LCs exhibited the best matching with the emission spectrum (Fig. 4a). Consequently, **R1** or **S1** was placed behind the 4-MUP aqueous solution, and the CPL performance of the entire composite system was tested. The results fully met expectations, as shown in Fig. 4b, the CPL spectra displayed excellent symmetry after the inclusion of **R1** and **S1**. Moreover, the luminescence dissymmetry factors of circularly polarized light emitted by the composite system reached the theoretical values of +2 and −2, respectively (Supplementary Table S5, entry 1-2; Fig. 4c and Supplementary Fig. S37). With this result, the CPL properties of a series of achiral molecules in aqueous solution, combined with N*-LCs, were tested using this strategy. Including disodium *N*-(ethoxycarbonylmethyl)-6-methoxyquinolinium bromide (MQAE), 6-methoxy-*N*-(3-sulfopropyl)quinolinium (SPQ), 4,4′-bis(2-sulfostyryl) biphenyl (CBS), lucifer yellow CH dipotassium salt (LY), rhodamine 6G (R6G), sulforhodamine B (SRB) and rhodamine B (RB), as shown in Fig. 3. The fluorescence emission spectra of these molecules are shown in Supplementary Fig. S34. As examples, Fig. 4a demonstrates the matching of the fluorescence emission peaks of CBS, LY, R6G, RB, and reflection spectra of *S*-type N*-LC. Therefore, by employing this strategy, Fig. 4b, c illustrates that the CPL generated from these solutions-N*-LCs composite system exhibited excellent mirror symmetry and dissymmetry factors exceeding ±1.5, with some reaching the theoretical maximum of ±2. SPQ, MQAE and SRB exhibited the same results with others (Supplementary Table S5, Supplementary Figs. S37–S39), thereby confirming the feasibility of this strategy.

To verify the universality of this strategy, further investigations were extended to a range of luminescent organic-solvent soluble molecules (Fig. 3). From blue-light to red-light, including fluorescent molecules such as 9,10-bis[*N*,*N*-di-(p-tolyl)-amino]anthracene (TTPA), rubrene, and 4-(dicyanomethylene)-2-methyl-6-(4-dimethylaminostyryl)-4H-pyran (DCM); phosphorescent molecules such as Iridium(III) bis(4-(4-tert-butylphenyl) thieno[3,2-c] pyridinato-*N*,C2′) acetylacetonate (PO-01-TB) and Ir(mphmq)$_2$tmd (REP); thermally activated delayed fluorescence (TADF) molecules such as 9,9′-(sulfonylbis(4,1-phenylene))bis(9H-carbazole) (Cz-DPS), 9,9′-(sulfonylbis(4,1-phenylene))bis(3,6-di-tert-butyl-9H-carbazole) (tBuCz-DPS), 10,10′-(sulfonylbis(4,1-phenylene))bis(9,9-dimethyl-9,10-dihydroacridine) (DMAC-DPS), 10-(4-(4,6-diphenyl-1,3,5-triazin-2-yl)phenyl)-9,9-dimethyl-9,10-dihydroacridine (DMAC-TRZ), and 10-(phenanthridin-6-yl)-10H-phenoxazine (CPT-PXZ); multiple resonance-induced TADF (MR-TADF) molecules such as 2,12-di-tert-butyl-5,9-bis(4-(*tert*-butyl)phenyl)-5,9-dihydro-5,9-diaza-13b-boranaphtho[3,2,1-de]anthracene (BNC), and DtBuCzB (TBN). Figure 4d–f using Cz-DPS, TBN, TTPA, PO-01-TB and REP as examples, demonstrates the matching of the fluorescence emission spectra of them with the corresponding reflection spectra of the *S*-type N*-LC. Similarly, by placing the matching N*-LC behind the toluene solution of these molecules, the composite system successfully achieved high-performance circularly polarized luminescence. The CPL spectra exhibited mirror symmetry, with $|g_{lum}|$ values greater than 1.6, and even reaching the theoretical maximum of 2. Beyond these five examples, other molecules soluble in organic solvents that were selected in this study also demonstrated high-performance CPL when using the same strategy in toluene solution (Supplementary Table S6, Supplementary Figs. S40–S43). These results collectively demonstrate the feasibility, universality, simplicity, and robustness of this strategy for generating CPL with high $|g_{lum}|$ values in solution. To study the effect of the incorporation of luminescent molecules on N*-LC, Cz-DPS was doped into **R1** at three different ratios (1.4 wt%, 1.8 wt%, and 2.2 wt%). As shown in Supplementary Fig. S46, after doping Cz-DPS into **R1**, the g_{lum} values decreased from 2.0 (when Cz-DPS was separated from **R1**, Supplementary Table S6) to 1.3-1.4. This indicates that the doping of luminescent molecules has disrupted the ordered assembly of N*-LC, thereby reducing the g_{lum} values.

White-light circularly polarized luminescence has recently garnered significant attention from both academia and industry due to its broad application potential in photoelectric devices, optical sensors, information storage and optical anticounterfeiting[53]. Achieving white-light CPL emission typically requires a mixture of either chiral molecules emitting the three primary colors or two complementary-color chiral molecules[54–57]. In this work, two mixed solutions were successfully constructed using complementary-color emitters, one in aqueous and the other in organic toluene solvents. Specifically, blue-emitting MQAE and yellow-emitting R6G were combined in the aqueous system, while blue-emitting DMAC-DPS and yellow-emitting PO-01-TB were mixed in the organic system. The fluorescence emission spectra of both systems exhibit dual peaks, with the aqueous system emitting at 455 nm and 564 nm (Fig. 4g), and the organic system emitting at 468 nm and 559 nm (Fig. 4j). Their CIE coordinates are (0.31, 0.34) and (0.31, 0.35), respectively (Fig. 4h, k), both falling within the white-light region, thus demonstrating the successful preparation of white-light solutions. Building on the N*-LC strategy proposed in this article, a method to achieve white-light CPL with high g_{lum} values was designed by placing two N*-LCs, each selectively reflecting blue and yellow wavelengths, behind the white-light solutions. The experimental results confirm this approach. For the aqueous system, white-light CPL was generated with g_{lum} values reaching +1.9 (*R*), −1.8 (*S*) at 455 nm, and +2.0 (*R*) and −1.9 (*S*) at 564 nm (Supplementary Table S7, Supplementary Fig. S44). Similarly, for the organic system, g_{lum} values reached +1.6 (*R*) and −1.5 (*S*) at 468 nm, and +1.6 (*R*) and −1.8 (*S*) at 559 nm (Table S7, Supplementary Fig. S44). These results further validate the universality and versatility of the N*-LC strategy for achieving high g_{lum} values circularly polarized light in solution. Moreover, these results also indicate that when achiral luminescent molecules are separated from N*-LCs, the further enhancement of the $|g_{lum}|$ can be achieved.

Logic gates

One of the key advantages of luminescent solution systems over solid-state systems is their ability to achieve tunable color changes, making them suitable for applications such as probes. For instance, reversible color modulation can be achieved through acid–base regulation. When an appropriate N*-LC is placed behind the achiral solution, the strategy based on the selective reflection-transmission mechanism of

https://doi.org/10.1038/s41467-025-58355-8

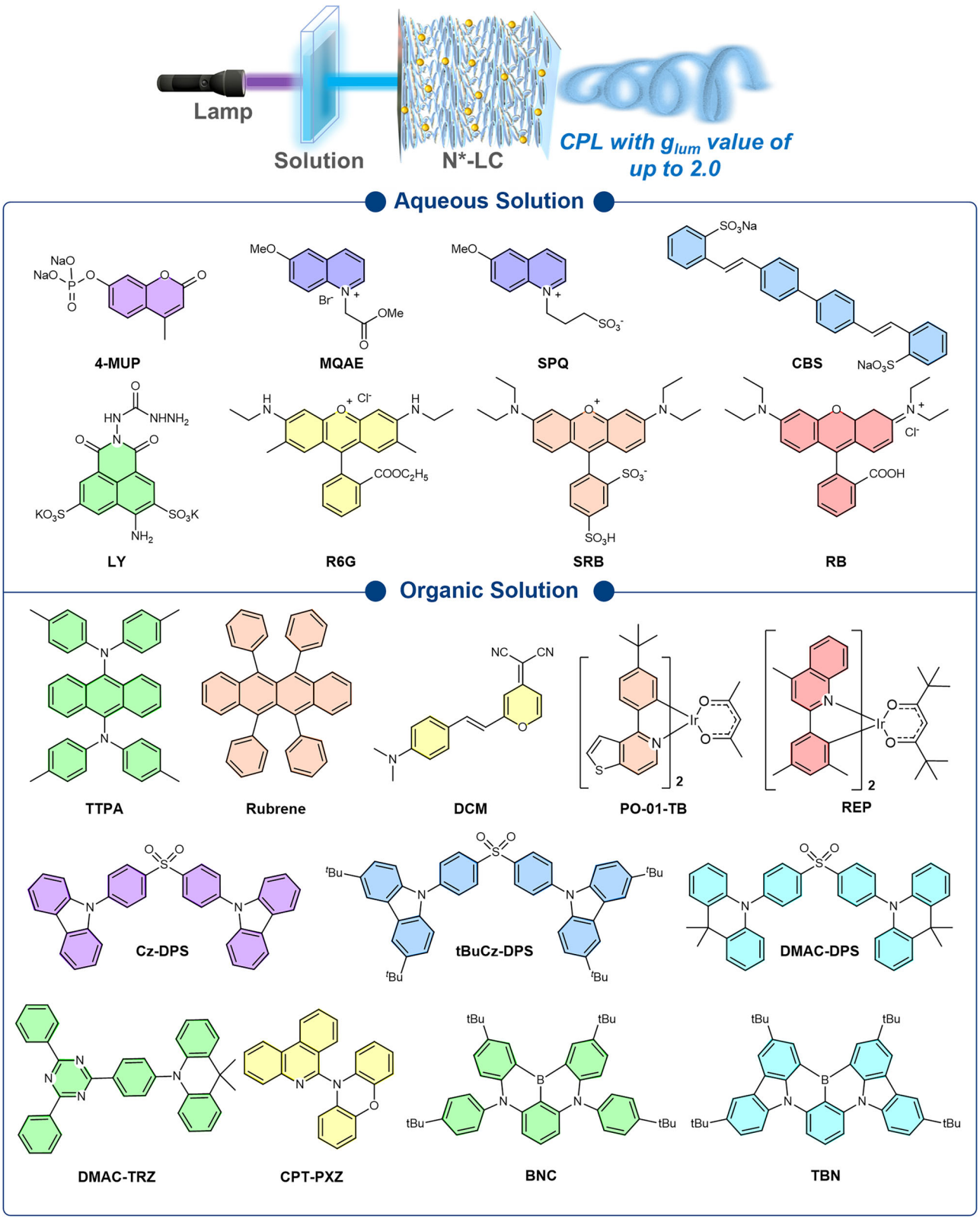

Fig. 3 | Strategy diagram and molecular structure. Scope of achiral luminescent molecules tested in this study.

the liquid crystal, as proposed in this study, allows acid and base stimuli to function as CPL switches. In this study, a fluorenyl derivative with two isoquinoline substituents, 5,5′-(9,9-dihexyl-9H-fluorene-2,7-diyl)diisoquinoline (F6IQ), was synthesized. As shown in Supplementary Fig. S36, the fluorescence emission of a 300 μL 1×10^{-2} M toluene solution of F6IQ occurs at 390 nm, exhibiting a blue color. Upon the addition of 50 μL trifluoroacetic acid (TFA), the nitrogen on the isoquinoline group is protonated (Supplementary Figs. S30–S33), causing the fluorescence emission of the F6IQ + TFA system to shift to 550 nm, changing from blue to yellow. Subsequently, the addition of 150 μL

https://doi.org/10.1038/s41467-025-58355-8

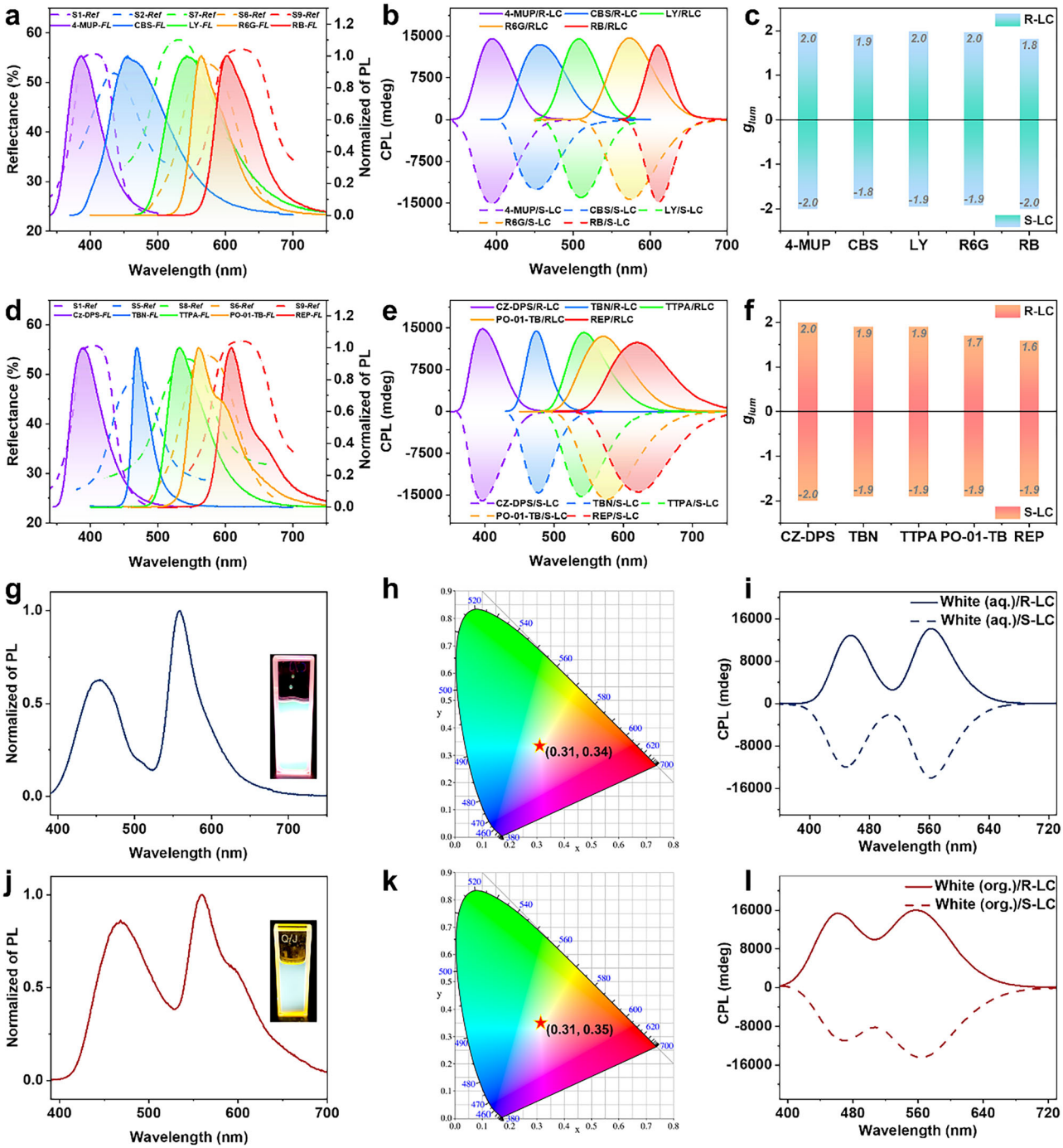

Fig. 4 | Spectrum of systems. a Emission spectra of 4-MUP, CBS, LY, R6G, RB and reflection spectra of various N*-LCs. **b** CPL spectra and **c** g_{lum} values of 4-MUP, CBS, LY R6G and RB in aqueous solution with N*-LC. **d** Emission spectra of CZ-DPS, TBN, TTPA, Rubrene, REP and reflection spectra of various N*-LCs. **e** CPL spectra and **f** g_{lum} values of CZ-DPS, TBN, TTPA, Rubrene and REP in toluene solution with N*-LC. **g** Fluorescence spectra (Illustration: fluorescence image of white luminescence aqueous solution). **h** CIE coordinates and **i** CPL spectra of white luminescence aqueous solution. **j** Fluorescence spectra (Illustration: fluorescence image of white luminescence organic solution). **k** CIE coordinates and **l** CPL spectra of white luminescence aqueous solution.

triethylamine (Et_3N) to the F6IQ + TFA system results in the fluorescence emission shifting back to 390 nm, restoring the blue color. This demonstrates that the fluorescence of F6IQ exhibits a distinct reversible acid-base response.

As shown in Fig. 5a, b, the CPL signal of F6IQ in toluene was successfully induced by **R2** and **S2**, with a g_{lum} value of 1.9 and −2.0 at 397 nm (Fig. 5b, c). Upon addition of TFA to the toluene solution, the DC signal shifted from 397 nm to 550 nm (Supplementary Fig. S45), consistent with the fluorescence emission results. However, influenced by the reflection of N*-LC, the CPL signal shifted to 460 nm (Fig. 5b). Without altering the N*-LC, the g_{lum} value of F6IQ-TFA decreased to 0.5 and −0.5 at 460 nm, 0.03 and −0.06 at 550 nm (Fig. 5d). Compared to the original CPL signal at 397 nm (g_{lum} = 1.9 and −2.0), it can be concluded that the CPL signal was "turned off" by the acid treatment. Subsequently, upon addition of Et_3N, the fluorescence emission peak returned to its original position at 397 nm, and the CPL signal was restored with an intensity similar to the initial state (g_{lum} = 2.0 and −1.9, Fig. 5b, c). Based on the CPL switching behavior of F6IQ described

https://doi.org/10.1038/s41467-025-58355-8

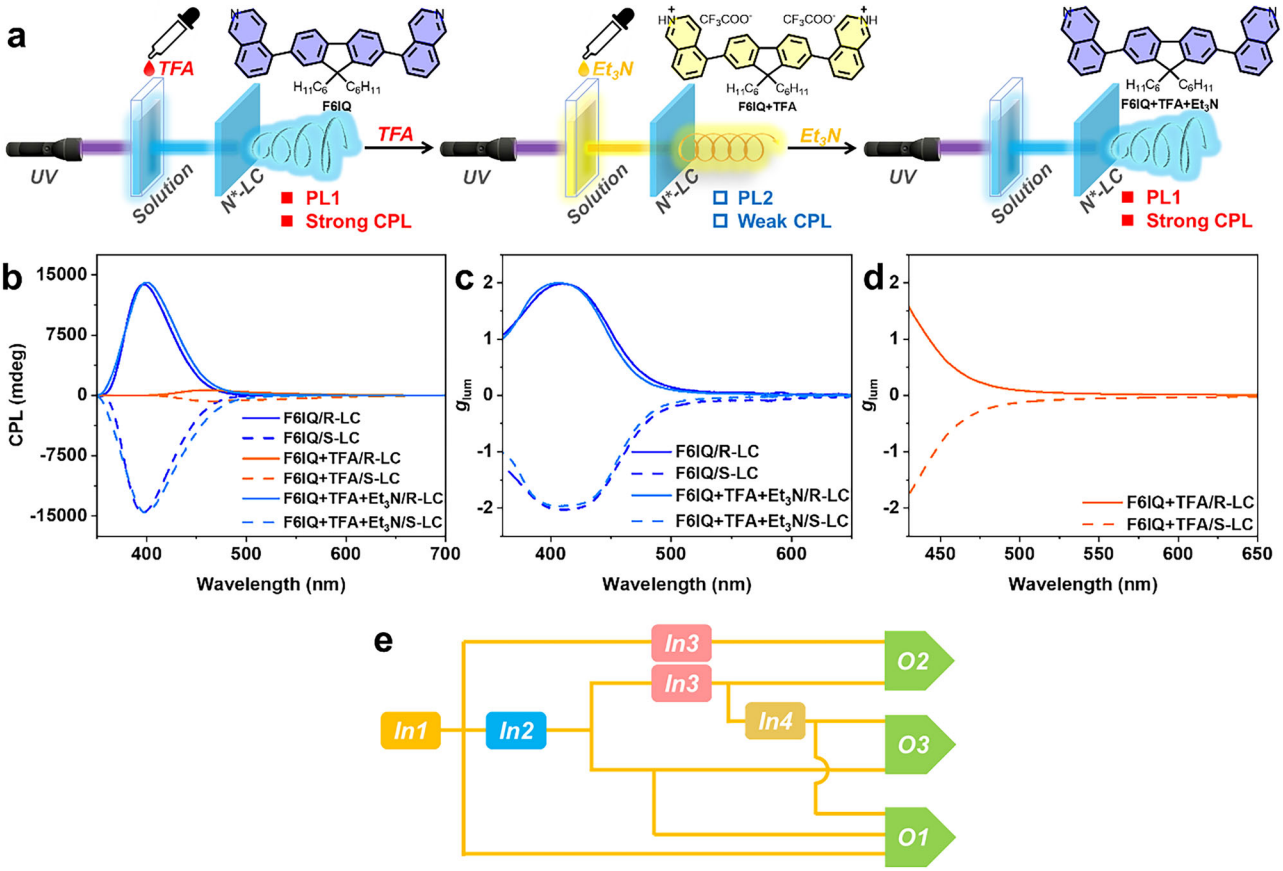

Fig. 5 | Reversible acid-base response and logic gate. a Schematic diagram of the CPL switch achieved by utilizing the reversible acid-base response of the solution and the selective reflection-transmission mechanism of N*-LC. **b** CPL spectra of F6IQ, F6IQ + TFA, F6IQ + TFA + Et_3N in toluene with N*-LC **R2** and **S2**. **c** g_{lum} value of F6IQ + TFA + Et_3N in toluene with N*-LC **R2** and **S2**. **d** g_{lum} value of F6IQ + TFA in toluene with N*-LC **R2** and **S2**. **e** The schematic diagram of the designed logic gate.

Table 1 | Truth table of the designed logic gate

INPUT				OUTPUT		
In1 UV	In2 N*-LC	In3 TFA	In4 Et_3N	O1 PL1	O2 PL2	O3 CPL
1	0	0	0	1	0	0
1	0	1	0	0	1	0
1	1	0	0	1	0	1
1	1	1	0	0	1	0
1	1	1	1	1	0	1

above, a molecular logic gate with multi-output capabilities was designed using acid–base regulation of F6IQ and selective reflection-transmission mechanism. To effectively construct the proposed logic circuit, the freshly prepared toluene solution of F6IQ (1×10^{-2} M, 300 μL) was defined as the initial state of the logic gate. Four inputs were specified: ultraviolet light (330 nm; INPUT 1), N*-LC (**R2**/**S2**; INPUT 2), TFA (50 μL; INPUT 3), and Et_3N (150 μL; INPUT 4). The absence or presence of stimuli was assigned as logical inputs "0" and "1" respectively. Outputs O1, O2, and O3 were defined as the presence of fluorescence at 397 nm, fluorescence at 460 nm, and CPL activity, respectively. The absence and presence of a signal were assigned as logical outputs "0" and "1." For fluorescence signals at 397 nm or 460 nm, the output was defined as "1." Similarly, the presence of a CPL signal was assigned as "1". The truth table and schematic diagram of the logic gate are shown in Table 1 and Fig. 5e. For example, when 330 nm excitation (INPUT 1 = 1), placement of N*-LC behind the solution (INPUT 2 = 1), addition of TFA (INPUT 3 = 1), and addition of Et_3N (INPUT 4 = 1) were applied, the resulting output included CPL activity with 397 nm fluorescence. The corresponding outputs for O1–O3 were 1, 0, and 1, respectively. Thus, the designed logic gate operates under various external inputs and outputs multiple types of information in response to stimuli. This model provides an approach for developing optical logic devices.

Discussion

In summary, this study develops a general and robust strategy for achieving full-color and white circularly polarized luminescence of achiral organic molecules in solutions using N*-LC materials doped with *R*/*S*-5011 and SLC1717. Specifically, this strategy involves placing the N*-LC behind the solution to convert unpolarized light emitted by the solution into CP light through the selective reflection and transmission of N*-LC. The resulting CP light generated by the composite system demonstrates $|g_{lum}|$ values exceeding 1.5, or even achieving 2.0. This approach is applicable to both aqueous and organic solution systems; accommodating various types of emitters, including fluorescent, phosphorescent, TADF, and MR-TADF molecules. At the molecular level, this strategy avoids the complex chiral separation and purification processes required for chiral organic emitters. At the N*-LC level, this strategy avoids the disruption of the highly ordered chiral assembly of the N*-LCs caused by the addition of luminescent molecules. Additionally, at the material level, these N*-LC materials are simpler to prepare, more cost-effective, and highly tunable compared to traditional optical components that rely on polarizers and quarter-wave plates. These advantages underscore the potential of this strategy for large-scale applications. Moreover, by exploiting the tunable acid–base responsiveness of the solution and the selective reflection-transmission mechanism of N*-LCs, switchable CPL features were

employed to design logic gates. This general and robust strategy provides inspiration and design concepts for constructing circularly polarized luminescence materials.

Methods

Materials

Except CPT-PXZ and F6IQ, all reagents were purchased from commercial providers without further purification. SLC1717, was bought from the Nanjing Ningcui Optical Technology Co., Ltd. Chiral dopant, R/S-5011 (99%), was bought from the Nanjing Sanjiang New Materials R & D Co., Ltd. 4-MUP (98%) and MQAE (99%) were purchased from MACKLIN. SPQ (97%) and SRB (95%) were purchased from Bide Pharmatech Co.,Ltd. CBS (97%) and R6G (95%) were purchased from Aladdin. LY (99%) was purchased from Leyan. RB (T.P.), NaH (60% dispersion in mineral oil), phenoxazine (98%), 6-chlorophenanthridine (95%) and 5-bromoisoquinoline (97%) were purchased from Innochem. TTPA, Rubrene (98%), DCM (99%) and 2,7-bis(4,4,5,5-tetramethyl-1,3,2-dioxaborolan-2-yl)-9,9-dihexylfluorene (98%) were purchased from Alfa Aesar. PO-01-TB (99%), REP (99%), Cz-DPS (99%), tBuCz-DPS (99%) and DMAC-DPS (99%) were purchased from Yurisolar. DMAC-TRZ (99%), BNC (99%) and TBN (99%) were purchased from FRST. $Pd(PPh_3)_4$ (99%) was purchased from J&K.

Preparation of N*-LC

R1: SLC1717 (370 μL), *R*-5011 (10.69 mg) and dichloromethane (5 mL) were added to a 20 mL sample bottle. After ultrasonic treatment for 5 min, the mixture was heated and dried with a hot stage at 80 °C to obtained doped N*-LC. The doping concentration was 28.89 g L^{-1}. The preparation process of other N*-LC (**R2-R9, S1-S9**) were the same as that of **R1**. The amounts of *R*/*S*-5011, SLC1717 and the doping concentration of the corresponding N*-LC were shown in Supplementary Table S1 and S2. Subsequently, these N*-LCs are encapsulated between two 1.5 × 1.5 cm quartz plates for further testing.

Spectroscopic measurements

UV-vis, reflection and transmission measurement were conducted on a PerkinElmer® UV/Vis/NIR spectrometer (Lambda 950). CD measurement was conducted on a JASCO J810 spectropolarimeter. POM measurement was recorded on Leica DM2700M upright materials microscope. CPL spectra together with g_{lum} values are measured and recorded at room temperature on JASCO CPL-300 spectrophotometer. ^{1}H-NMR and ^{13}C-NMR were recorded on AVIII 400 MHz and 500 MHz NMR spectrometers using $CDCl_3$ and THF-d_8 as solvent. HR-MS was measured on the Thermo Fisher® Exactive high resolution LC-MS spectrometer. Fluorescence spectra and transient PL decay characteristics were carried out using an Edinburgh Instruments FLS 1000 spectrometer.

Synthesis and characterization of CPT-PXZ

Under Ar atmosphere, NaH (0.25 g, 6.2 mmol) was added to a solution of phenoxazine (1.17 g, 5.6 mmol) in dry THF (50 mL). After the resulting mixture stirred at 70 °C for 30 min, 6-chlorophenanthridine (1.00 g, 4.7 mmol) was added to the mixture. The resulting mixture was refluxed for 24 h. Cooling to room temperature, the pure product was precipitated by filtering and recrystallization. Finally, the pure compound was obtained as a yellow-green solid (1.13 g, 75%). ^{1}H NMR (500 MHz, $CDCl_3$): δ 8.73 (d, *J* = 8.3 Hz, 1H), 8.69–8.65 (m, 1H), 8.41 (d, *J* = 8.2 Hz, 1H), 8.27–8.23 (m, 1H), 7.91 (ddd, *J* = 8.2, 6.9, 1.3 Hz, 1H), 7.80 (tt, *J* = 7.1, 5.2 Hz, 2H), 7.69–7.62 (m, 1H), 6.84–6.77 (m, 2H), 6.73–6.67 (m, 2H), 6.56–6.48 (m, 2H), 5.96–5.90 (m, 2H). ^{13}C NMR (126 MHz, $CDCl_3$): δ 151.0, 144.1, 144.0, 136.0, 133.1, 131.8, 130.3, 129.1, 128.4, 128.1, 126.6, 124.6, 123.4, 122.8, 122.2, 122.0, 115.8, 113.8. HRMS (ESI) (*m/z*): calcd. for $C_{25}H_{17}N_2O$ $[M+H]^+$ 361.1337, found: 361.1335. Transient PL decay spectra of CPT-PXZ was shown in Supplementary Fig. S35.

Synthesis and characterization of F6IQ

Under N_2 atmosphere, 2,7-bis(4,4,5,5-tetramethyl-1,3,2-dioxaborolan-2-yl)-9,9-dihexylfluorene (0.31 g, 0.53 mmol), 5-bromoisoquinoline (0.35 g, 3eq), $Pd(PPh_3)_4$ (0.06 mg, 0.1 eq), K_2CO_3 (0.37 g, 5eq), toluene (16 mL), EtOH (16 mL) and H_2O (8 mL) were added into a 100 mL Schlenk tube. After the resulting mixture stirred at 85 °C for 24 h and cooling to room temperature, the mixture was extracted with ethyl acetate, dried and concentrated to get hold of the crude product. The crude product was purified by column chromatography on silica gel (petroleum ether: ethyl acetate = 8:1 as the mobile phase) to afford F6IQ as a white solid (0.24 g, 77%). ^{1}H NMR (400 MHz, THF-d_8): δ 9.19 (s, 2H), 8.34 (d, *J* = 5.9 Hz, 2H), 7.94 (d, *J* = 8.0 Hz, 2H), 7.87 (d, *J* = 7.7 Hz, 2H), 7.69–7.63 (m, 4H), 7.63–7.56 (m, 2H), 7.48 (s, 2H), 7.41 (d, *J* = 7.7 Hz, 2H), 2.10–1.96 (m, 4H), 1.05 (d, *J* = 12.9 Hz, 13H), 0.85–0.72 (m, 4H), 0.67 (t, *J* = 6.7 Hz, 6H). ^{13}C NMR (101 MHz, THF-d_8): δ 152.2, 141.4, 140.5, 139.2, 134.9, 131.5, 130.2, 129.8, 129.7, 127.9, 127.6, 127.5, 125.5, 120.9, 118.84, 118.78, 56.3, 41.0, 32.5, 30.6, 23.4, 14.4. HRMS (ESI) (*m/z*): calcd. for $C_{43}H_{45}N_2$ $[M+H]^+$ 589.3577, found: 589.3599.

Preparation of solution

All aqueous solutions used deionized water as the solvent. Except for R6G and SRB, all aqueous solutions and F6IQ for logic gate were configured according to the concentration of 1×10^{-2} M. The light cannot completely penetrate the solution at the concentration of 1 $\times 10^{-2}$ for R6G and SRB, so for R6G and SRB, it is changed to the concentration of 1×10^{-3}. All organic solutions used toluene as the solvent and were configured with the concentration of 5×10^{-3}.

Data availability

All data supporting this study including detailed methods and experimental details, photophysical properties studies, are available in Manuscript and Supplementary information. All data are available upon request Source data are provided with this paper.

References

1. Riehl, J. P. et al. Circularly polarized luminescence spectroscopy. *Chem. Rev.* **86**, 1–16 (1986).
2. Brittain, H. G. Excited-state optical activity, 1987–1995. *Chirality* **8**, 357–363 (1996).
3. Song, F. et al. Circularly polarized luminescence from AIEgens. *J. Mater. Chem. C* **8**, 3284–3301 (2020).
4. Brandt, J. R. et al. Circularly polarized phosphorescent electroluminescence with a high dissymmetry factor from PHOLEDs based on a platinahelicene. *J. Am. Chem. Soc.* **138**, 9743–9746 (2016).
5. Maeda, H. et al. Chemical-stimuli-controllable circularly polarized luminescence from anion-responsive π-conjugated molecules. *J. Am. Chem. Soc.* **133**, 9266–9269 (2011).
6. Guo, Q. et al. Multimodal-responsive circularly polarized luminescence security materials. *J. Am. Chem. Soc.* **145**, 4246–4253 (2023).
7. Shen, P. C. et al. Switchable dual circularly polarized luminescence in through-space conjugated chiral foldamers. *Angew. Chem. Int. Ed.* **63**, e202407605 (2024).
8. Sherson, J. F. et al. Quantum teleportation between light and matter. *Nature* **443**, 557–560 (2006).
9. Imai, Y. et al. A smart sensing method for object identification using circularly polarized luminescence from coordination-driven self-assembly. *Angew. Chem. Int. Ed.* **57**, 8973–8978 (2018).
10. Shuvaev, S. et al. Monitoring of the ADP/ATP ratio by induced circularly polarised europium luminescence. *Angew. Chem. Int. Ed.* **57**, 7488–7492 (2018).
11. Zhang, Y. et al. Circularly polarized luminescence in chiral materials. *Matter* **5**, 837–875 (2022).
12. Li, M. et al. Advances in circularly polarized electroluminescence based on chiral TADF-active materials. *Org. Chem. Front.* **9**, 6441–6452 (2022).

13. Wan, S.-P. et al. Advances in circularly polarized luminescent materials based on axially chiral compounds. *J. Photochem. Photobio. C: Photochem. Rev.* **50**, 100500 (2022).
14. Zhang, D.-W. et al. Recent advances in circularly polarized electroluminescence based on organic light-emitting diodes. *Chem. Soc. Rev.* **49**, 1331–1343 (2020).
15. Tan, K.-K. et al. Self-assembled chiral polymers exhibiting amplified circularly polarized electroluminescence. *Angew. Chem. Int. Ed.* **63**, e202412283 (2024).
16. Zhao, W.-L. et al. Chiral co-assembly based on a stimuli-responsive polymer towards amplified full-color circularly polarized luminescence. *Angew. Chem. Int. Ed.* **64**, e202416863 (2025).
17. Yang, S. et al. Circularly polarized luminescence polymers: From design to applications. *Coord. Chem. Rev.* **485**, 215116 (2023).
18. Luo, X.-Y. et al. Metal-organic materials with circularly polarized luminescence. *Coord. Chem. Rev.* **468**, 214640 (2022).
19. Yang, X. et al. Recent progress of circularly polarized luminescence materials from Chinese perspectives. *CCS Chem.* **5**, 2760–2789 (2023).
20. Kitzmann, W. R. et al. Fundamentals, advances, and artifacts in circularly polarized luminescence (CPL) spectroscopy. *Adv. Mater.* **35**, 2302279 (2023).
21. Bispo-Jr, A. G. et al. Perspectives and challenges in circularly polarized luminescence of lanthanide(III) complexes: From solution-based systems to solid-state applications. *Coord. Chem. Rev.* **523**, 216279 (2025).
22. Furlan, F. et al. Chiral materials and mechanisms for circularly polarized light-emitting diodes. *Nat. Photonics* **18**, 658–668 (2024).
23. Takaishi, K. et al. Helical oligonaphthodioxepins showing intense circularly polarized luminescence (CPL) in solution and in the solid state. *Chem. Euro. J.* **23**, 9249–9252 (2017).
24. Jiang, Z. et al. Easily accessible axial chiral binaphthalene-triarylborane dyes displaying intense circularly polarized luminescence both in solution and in solid-state. *Dyes. Pigm.* **175**, 108168 (2020).
25. Sheng, Y. et al. Reversal circularly polarized luminescence of aie-active chiral binaphthyl molecules from solution to aggregation. *Chem. Euro. J.* **21**, 13196–13200 (2015).
26. Sawai, M. et al. Circularly polarized luminescence (CPL) characteristics of hydrophobic pyrene derivatives/γ-cyclodextrin (γ-CD) complexes in aqueous solution dissolved by grinding. *J. Incl. Phenom. Macrocycl. Chem.* **102**, 133–142 (2022).
27. Grell, M. et al. Polarized luminescence from oriented molecular materials. *Adv. Mater.* **11**, 895–905 (1999).
28. Geelhaar, T. et al. 125 years of liquid crystals—a scientific revolution in the home. *Angew. Chem. Int. Ed.* **52**, 8798–8809 (2013).
29. Fischer, P. et al. Nonlinear optical spectroscopy of chiral molecules. *Chirality* **17**, 421–437 (2005).
30. Wang, X. et al. Three-level chirality transfer and amplification in liquid crystal supramolecular assembly for achieving full-color and white circularly polarized luminescence. *Adv. Mater.* **37**, 2412805 (2024).
31. Li, Y. et al. Photodynamic chiral molecular switches with thermal stability: From reflection wavelength tuning to handedness inversion of self-organized helical superstructures. *Angew. Chem. Int. Ed.* **52**, 13703–13707 (2013).
32. Zheng, Z.-G. et al. Three-dimensional control of the helical axis of a chiral nematic liquid crystal by light. *Nature* **531**, 352–356 (2016).
33. Bisoyi, H. K. et al. Light-driven liquid crystalline materials: From photo-induced phase transitions and property modulations to applications. *Chem. Rev.* **116**, 15089–15166 (2016).
34. Chen, Y. H. et al. Dynamic circularly polarized luminescence with tunable handedness and intensity enabled by achiral dichroic dyes in cholesteric liquid crystal medium. *Adv. Mater.* **34**, 2202309 (2022).
35. Zhang, M. J. et al. Amplifying inorganic chirality using liquid crystals. *Nanoscale* **14**, 592–601 (2022).
36. Li, M. et al. Light-reconfiguring inhomogeneous soft helical pitch with fatigue resistance and reversibility. *J. Am. Chem. Soc.* **144**, 20773–20784 (2022).
37. Wu, Y. et al. Rational design of circularly polarized luminescent aggregation-induced emission luminogens (AIEgens): Promoting the dissymmetry factor and emission efficiency synchronously. *ACS Mater. Lett.* **2**, 505–510 (2020).
38. San Jose, B. A. et al. Dynamic switching of the circularly polarized luminescence of disubstituted polyacetylene by selective transmission through a thermotropic chiral nematic liquid crystal. *Angew. Chem. Int. Ed.* **53**, 10641–10644 (2014).
39. Liu, S. et al. Circularly polarized perovskite luminescence with dissymmetry factor up to 1.9 by soft helix bilayer device. *Matter* **5**, 2319–2333 (2022).
40. Han, J. et al. Full-color tunable circularly polarized luminescent nanoassemblies of achiral aiegens in confined chiral nanotubes. *Adv. Mater.* **29**, 1606503 (2017).
41. Song, F. et al. Tunable circularly polarized luminescence from molecular assemblies of chiral AIEgens. *Mater. Chem. Front.* **3**, 1768–1778 (2019).
42. Yan, J. et al. Chiroptical resolution and thermal switching of chirality in conjugated polymer luminescence via selective reflection using a double-layered cell of chiral nematic liquid crystal. *Adv. Funct. Mater.* **27**, 1604529 (2017).
43. Zheng, H. et al. Uncovering the circular polarization potential of chiral photonic cellulose films for photonic applications. *Adv. Mater.* **30**, 1705948 (2018).
44. Wang, X. et al. Liquid crystals doped with chiral fluorescent polymer: Multi-color circularly polarized fluorescence and room-temperature phosphorescence with high dissymmetry factor and anti-counterfeiting application. *Adv. Mater.* **35**, 2304405 (2023).
45. Zhong, H. et al. Matching rule" for generation, modulation and amplification of circularly polarized luminescence. *Acc. Chem. Res.* **57**, 1188–1201 (2024).
46. Luo, J. et al. Ultrastrong circularly polarized luminescence triggered by the synergistic effect of chiral coassembly and selective reflective cholesteric liquid crystal film. *ACS Mater. Lett.* **6**, 2957–2963 (2024).
47. Xu, M. et al. Exploring the circular polarization capacity from chiral cellulose nanocrystal films for a photo-controlled chiral helix of supramolecular polymers. *Angew. Chem. Int. Ed.* **61**, e202117042 (2022).
48. Jia, S. et al. Dual-direction circularly polarized luminescence materials with on-demand handedness and superior flexibility. *Adv. Funct. Mater.* **34**, 2410206 (2024).
49. Zhu, Y. et al. Nematic liquid crystals induce and amplify the circularly polarized luminescence of chiral TADF emitters. *J. Mater. Chem. C* **10**, 5065–5069 (2022).
50. Shang, W. et al. Self-assembly of macrocyclic triangles into helicity-opposite nanotwists by competitive planar over point chirality. *Angew. Chem. Int. Ed.* **61**, e202210604 (2022).
51. Guo, C.-H. et al. Chiral co-assembly with narrowband multi-resonance characteristics for high-performance circularly polarized organic light-emitting diodes. *Adv. Mater.* **36**, 2406550 (2024).
52. Wu, Y. et al. Liquid crystal assembly for ultra-dissymmetric circularly polarized luminescence and beyond. *J. Am. Chem. Soc.* **145**, 12951–12966 (2023).
53. Zhao, P. et al. Single-molecule white circularly polarized photoluminescence and electroluminescence from dual-emission enantiomers. *Angew. Chem. Int. Ed.* **63**, e202409020 (2024).
54. Tang, X. et al. All-fluorescence white organic light-emitting diodes exceeding 20% EQEs by rational manipulation of singlet and triplet excitons. *Adv. Funct. Mater.* **30**, 1910633 (2020).

55. Wang, Q. et al. Alleviating efficiency roll-off of hybrid single-emitting layer WOLED utilizing bipolar TADF material as host and emitter. *ACS Appl. Mater. Interfaces* **11**, 2197–2204 (2019).
56. Li, B. et al. Realizing efficient single organic molecular white light-emitting diodes from conformational isomerization of quinazoline-based emitters. *ACS Appl. Mater. Interfaces* **12**, 14233–14243 (2020).
57. Wang, R. et al. Solution-processed white organic light-emitting diodes with bi-component emitting layer based on symmetry blue spiro-sulfone derivative. *Org. Electron.* **71**, 24–30 (2019).

Acknowledgements

We thank the National Natural Science Foundation of China (92256304, 22122111), the Ministry of Science and Technology of China (2022YFA1204401), and Beijing National Laboratory for Molecular Sciences (BNLMS-CXXM-202105) for financial support.

Author contributions

C.-F.C. designed and directed the project. M.-J.J. and W.-L.Z. conducted the experiments and wrote the manuscript. M.L. was involved in the discussions and contributed to the manuscript preparation. All authors revised and finalized the manuscript.

Competing interests

The authors declare no competing interests.

Additional information

Supplementary information The online version contains supplementary material available at https://doi.org/10.1038/s41467-025-58355-8.

Correspondence and requests for materials should be addressed to Meng Li or Chuan-Feng Chen.

Peer review information *Nature Communications* thanks Yixiang Cheng, and the other, anonymous, reviewers for their contribution to the peer review of this work. A peer review file is available.